Microchimica Acta (2023) 190:419
https://doi.org/10.1007/s00604-023-05997-4

ORIGINAL PAPER

Computer-aided design of molecularly imprinted polymer reinforced by double hybrid monomers for selective purification of hydroxycamptothecin

Fang Nie[1,2,3,4] · Chunying Li[1,2,3,4] · Bin Qiao[1,2,3,4] · Junling Wang[1,2,3,4] · Yuan Gao[1,2,3,4] · Jie Liu[5] · Chunjian Zhao[1,2,3,4]

Received: 20 April 2023 / Accepted: 11 September 2023 / Published online: 28 September 2023

Abstract

A kind of hydroxycamptothecin (HCPT) hybrid molecularly imprinted polymer (AT/MA-HMIPs) with high selectivity and hard silicon skeleton was successfully prepared based on double hybrid monomers. The relationship between templates and functional monomers was studied through computer molecular simulation and experiments. Three single-monomer molecularly imprinted polymers were prepared as controls. The Langmuir isotherm and pseudo-second-order kinetic models were found to fit well with the adsorption results. The maximum adsorption capacity was 18.79 mg/g, and equilibrium was reached within 20 min. Moreover, it shows excellent selectivity (imprinting factor is 10.73) and good recoverability (after 10 adsorption-desorption cycles, the adsorption capacity only decreases by 7.75%) for HCPT. The purity of HCPT can reach 80.86% after being put into a solid phase extraction column and used in an actual sample, and the yield was 61.43%. This study lays the fundament for the development of excellent HCPT molecularly imprinted composites.

Keywords Hydroxycamptothecin · Selective adsorption · Molecularly imprinted polymers · Molecular simulation · Solid phase extraction

Introduction

Camptotheca acuminate Decne (*C. camptotheca*), also known as dry lotus tree, is a deciduous tree of the blueberry family and *Camptotheca* species, widely distributed in southern China [1]. *C. camptotheca* has been widely concerned by researchers because of its unique active substances, with alkaloids being of particular interest [2, 3]. Hydroxycamptothecin (HCPT) is an alkaloid with strong anticancer properties and low toxicity, selectively acting on the S phase of the cell cycle, inhibiting topoisomerase I, and interfering with DNA replication [4]. HCPT is used clinically to treat various cancers such as liver, stomach, lung, breast, and leukemia [5, 6]. The traditional extraction methods of HCPT in *C. camptotheca* mainly include decoction, percolation, reflux, Soxhlet extraction, ultrasonic extraction, and supercritical fluid extraction [1, 7]. Although they have some advantages, there are problems such as tedious steps, long extraction time, low extraction efficiency, large solvent consumption, and low purity. Therefore, a new and efficient extraction and purification technology is needed to better utilize medicinal plant resources.

✉ Chunying Li
lcy@nefu.edu.cn

✉ Chunjian Zhao
zcj@nefu.edu.cn

1 College of Chemistry, Chemical Engineering and Resource Utilization, Northeast Forestry University, Harbin 150040, China

2 Key Laboratory of Forest Plant Ecology, Ministry of Education, Northeast Forestry University, Harbin 150040, China

3 Engineering Research Center of Forest Bio-preparation, Ministry of Education, Northeast Forestry University, Harbin 150040, China

4 Heilongjiang Provincial Key Laboratory of Ecological Utilization of Forestry-based Active Substances, Harbin 150040, China

5 Hisun Pharmaceutical (Hangzhou) Co., Ltd., No 1, Road, Xukou Town, Fuyang District, Hangzhou 311404, China

Molecular imprinting technology (MIT) can form molecular imprinted polymers (MIPs) [8, 9]. It has many advantages, including selectivity and thermal and chemical stability, making it useful in various fields such as separation, medicine, and food [10, 11]. Hybrid molecularly imprinted polymers (HMIPs) are prepared by adding template molecules to rigid inorganic or inorganic-organic networks [12]. HMIPs are widely used in natural product separation, environmental monitoring, and food analysis due to their structural stiffness, thermal stability, large pores and specific surface area, and strong molecular recognition ability [13–15]. New hybrid functional monomers have been used in recent years to synthesize HMIPs, providing a feasible method to improve the polymer's mechanical strength, resistance to organic solvents, and permeability to the target [16, 17].

MIPs prepared from two or more functional monomers show better selectivity, stability, and adsorption capacity [18]. Because with the increase of functional monomer group diversity and the increase of interaction types between template molecules and bifunctional monomers, the complementary and synergistic effects of different monomers on molecular recognition increase, the diversity of the types of imprinting sites in the MIPs structure is enhanced [19–21]. Molecular simulation can be used to deeply explore the structure and behavior of molecules, so as to predict the physical and chemical properties of the system. It avoids the waste of manpower and material resources caused by a large number of repeated experiments in the past and also reduces the use of inevitably toxic reagents in chemical experiments as far as possible, which is more environmentally friendly [22–24].

In this work, computer molecular simulation was used to screen the most suitable functional monomers from nine different functional monomers. Dual hybrid monomers were used for the first time and were simulated using DFT. With HCPT as the template molecule, hybrid monomers AM-TEOSPI and MAA-APTES serve as both functional monomers; AT/MA-HMIPs were synthesized by surface imprinting, and the structural characteristics, adsorption capacity, selectivity, and reusability of AT/MA-HMIPs. It was used as an adsorbent to fill the solid phase extraction column, and its extraction conditions were optimized. Finally, it was used for solid phase extraction of HCPT in *C. camptotheca* seed powder, allowing for the separation and enrichment of HCPT. This provides a new strategy for extracting and purifying HCPT in complex samples.

Experimental

Materials and characterization

The materials and characterization are noted in the Supplementary information (Part S1).

Computer simulation of preferred functional monomers

The molecular models of the template molecule HCPT and the functional monomers MAA, acrylic acid (AA), AM, 2-vinylpyridine (2-VP), 4-vinylpyridine (4-VP), methyl methacrylate (MMA), vinyl acetate (VA), MAA-APTES, and AM-TEOSPI were established by Gaussian view 6.0 [25]. The geometric optimization, molecular electrostatic potential calculation, and natural population analysis (NPA) charge of the template molecule and the functional monomers were carried out by Gaussian 16 at the B3LYP 6-31G (d) and B3LYP def2-TZVP calculation levels with DFT-D3 dispersion correction [26, 27]. The spatial structure of the complex was optimized, and the binding energy was calculated (Eq. (1)). Finally, the independent gradient model (IGM) and gradient isosurface analysis were performed by using Multiwfn v.3.8 and VMD v.l.9.3 to analyze the region, magnitude, and type of force involved in the weak interaction in the system [28–30].

$$\Delta E = E_{\text{complex}} - E_{\text{HCPT}} - \sum E_{\text{monomer}} \quad (1)$$

E_{complex} (KJ/mol) is the energy of the most stable conception formed between HCPT and the monomers; E_{HCPT} (KJ/mol) is the energy of HCPT; E_{monomer} (KJ/mol) is the energy of the monomers in the most stable conformation.

Synthesis of AT/MA-HMIPs

The details of the preparation of MAA-APTES are described in the Supplementary information (Part S2) [31]. Preparation of AM-TEOSPI: Dissolve TEOSPI (2.5 mmol) in dichloromethane (10 mL), and stir at room temperature for 30 min. Add acrylamide (2.5 mmol) to the solution. Stir the solution for another 2 h until it is fully dissolved, remove the solvent by rotary evaporation, and then place it at 60 °C for vacuum drying for 24 h. The product AM-TEOSPI was characterized by FTIR (Supplementary Fig. S1), ^{1}H NMR (400 MHz, DMSO, 25 °C, TMS) (Supplementary Fig. S2), and MS. The quasi-molecular ion peak of AM-TEOSPI was ($[M+H]^{+}$) m/z = 341.15 (Supplementary Fig. S3).

Add HCPT (0.125 mmol), MAA-APTES (0.25 mmol), and AM-TEOSPI (0.25 mmol) into 30 mL methanol-chloroform (4:1, v/v), then ultrasonic treatment for 10 min and prepolymerization at 4 °C for 4 h. TEOS (0.4 mmol), EGDMA (5 mmol), and AIBN (60.0 mg) were added to the two solutions respectively. Nitrogen was deoxidized for 10 min, and these mixtures were polymerized at 60 °C for 24 h. After polymerization, vacuum dry, grind, and sieve. The obtained polymer was washed with methanol-acetic acid (9:1, v/v) through Soxhlet extraction to remove the template until the

template molecule could not be detected by HPLC. The acetic acid residue was removed by washing with methanol and then dried in a vacuum at 60 °C for 24 h to obtain hybrid molecular imprinted polymers (AT/MA-HMIPs).

The synthesis process of AT/MA-HNIPs is the same as that of AT/MA-HMIPs, except that no template molecules are added, and MAA, MAA-APTES, and AM-TEOSPI were used as separate functional monomers to obtain imprinted polymers (MAA-MIPs, MA-HMIPs, and AT-HMIPs) and non-imprinted polymers (MAA-NIPs, MA-HNIPs, and AT-HNIPs) as comparisons.

The adsorption test is detailed in Part S3 of the Supplementary information.

Application of AT/MA-HMIPs to adsorb HCPT in *C. camptotheca*

1.00 g of crushed *C. camptotheca* seed powder was added to a 100 mL triangular flask, followed by the addition of 40 mL of 70% ethanol. Ultrasonic extraction was performed at 40 °C for 30 min. The filter cake was washed and filtered with 5 mL 70% ethanol. The filtrate was diluted to 50 mL with 70% ethanol and shaken. Columns were packed and optimized according to Part S4 in the Supplementary information, and the target HCPT was then separated and purified from the *C. camptotheca* seed powder under optimized extraction conditions. The whole SPE procedure was also illustrated in Supplementary Fig. S4.

Results and discussion

Binding of template molecular and functional monomers

The structural optimization is described in the Supplementary information (Part S5). The nine functional monomers shown in Supplementary Fig. S6 all have reaction sites with hydrogen atoms on HCPT, but the values of negatively charged sites in MAA, AA, 2-VP, 4-VP, MMA, and VA that can form hydrogen bonds are small (−14.35, −15.83, −28.88, −36.78, −35.49, −31.90); the interaction with HCPT will be weak. The maximum point of the electrostatic potential of MAA, AA, and AM (+46.62, +47.02, +36.89) is close to its minimum point (−33.80, −33.07, −42.28), indicating that there is intra-molecular repulsion in the molecules near the maximum point, which is not conducive to the formation of hydrogen bonds. Both MAA-APTES and AM-TEOSPI have an ideal maximum (+40.94, +22.58, +22.50) and minimum sites (−40.05, −41.39, −41.45) and have the possibility of forming multiple hydrogen bonds with HCPT. Therefore, both of them can provide more active reaction sites and can be used as ideal functional monomers.

In the template molecule HCPT (Supplementary Fig. S7), the presence of carbonyl and tertiary amine nitrogen atoms in HCPT allows it to be located on both the highest occupied molecular orbital (HOMO) and lowest unoccupied molecular orbital (LUMO), indicating that it can function as both an electron donor and acceptor. It can be known from Supplementary Table S1 that HCPT is the main electron donor and the MAA-APTES has a greater ability to accept electrons [32]. The electrophilicity index (ω) calculated value of HCPT is higher than that of MAA-APTES and AM-TEOSPI, indicating that HCPT has a stronger electron acceptance ability. In summary, HCPT is the main electron acceptor, while MAA-APTES and AM-TEOSPI are electron donors [33].

All hydrogen bond lengths are between the general O-H single bond and the van der Waals radius (Supplementary Fig. S8). From Supplementary Table S2, it can be seen that compared to other traditional functional monomers and single functional monomers, the complex of HCPT-MA-AT has a lower binding energy (−46.315 kcal/mol) and a greater number of hydrogen bonds (14). The reason is that traditional functional monomers and single functional monomers have fewer active sites, relatively weak activity, and generate fewer hydrogen bonds. However, AM-TEOPI and MAA-APTES have more reaction sites and complementary functional groups that bind to the template molecule HCPT, and the combination of the two has a better effect and can be used as an ideal functional monomer for HCPT molecularly imprinted polymers.

From Fig. 1A, it can be seen that there are dense gradient peaks at the negative position, with a high *g* value, indicating that the hydrogen bond interaction between HCPT and AM-TEOSPI, MAA-APTES is stronger and the binding system of template molecules and functional monomers is stable [34]. At the same time, the gradient isosurface ($s = 0.5$ au) shown in Fig. 1B displays the location where the interaction occurs. The higher the blueness, the greater the dispersion attraction of the fragments and the stronger the dispersion attraction of the corresponding donor and recipient fragments. It is not difficult to see that the hydrogen bond and van der Waals interactions between HCPT and AM-TEOSPI, MAA-APTES systems are stronger. In addition, the bond lengths of HCPT with AM-TEOSPI and MAA-APTES are 1.77 Å and 1.80 Å, respectively. Strong hydrogen bonding can improve the adsorption performance of AT/MA-HMIPs.

As can be seen from Supplementary Fig. S9A, after adding AM-TEOSPI and MAA-APTES, the C=O stretching vibration of the HCPT moves from 1749.4 to 1734.2 cm^{-1}, while the C=N stretching vibration moves from 1654.9 to 1649.1 cm^{-1}, indicating that HCPT interacts with the two hybrid monomers [35]. At the same time, in

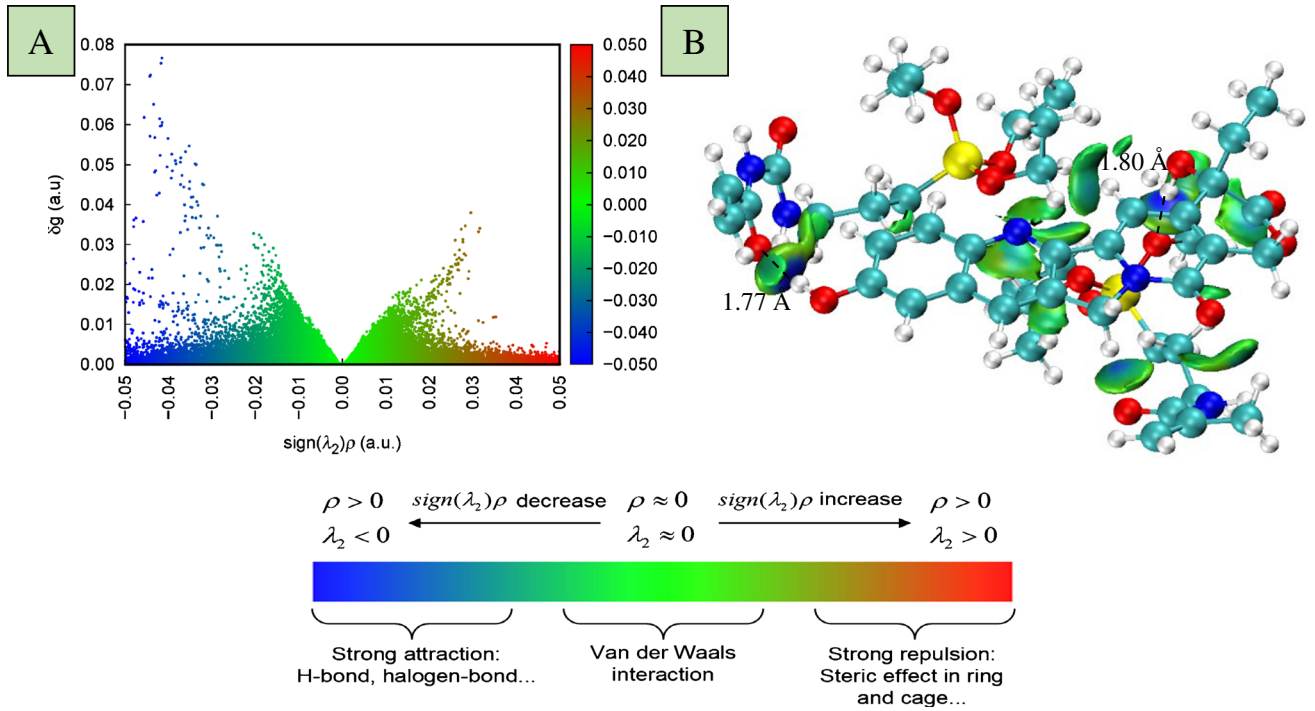

Fig. 1 Scatter diagram of the δg vs sign(λ_2)ρ (**A**) and the gradient isosurfaces (**B**, s = 0.5 au) for the optimal complex

the infrared spectrum of MAA-APTES, the wider peak formed in the 2980 cm^{-1} region is a stretching vibration peak of the enoic acid, and the absorption peak is significantly weakened after the interaction with HCPT, which is due to the association effect with HCPT. It can be explained that HCPT interacts with AM-TEOSPI and MAA-APTES.

As shown in Supplementary Fig. S9B, the maximum absorption wavelength slightly redshifted from 252.4 to 254.0 nm with the increase of the concentration of double hybrid monomer. According to the structure of the template molecule and the functional monomer, it can be inferred that there may be a hydrogen bond interaction between them, which changes the electron cloud density of the large π bond and the electron cloud distribution of the molecule on the benzene ring of HCPT, resulting in changes in the ultraviolet spectrum [34]. When the ratio of template and dual monomer is 1:6 and 1:8, the two hybrid functional monomers may self-bind; when the ratio of template and dual monomer is 1:1 and 1:2, a large number of HCPT may bind to each other through intermolecular forces, thus competing with the dual hybrid functional monomers AM-TEOSPI and MAA-APTES, reducing the binding site and weakening the imprinting effect [36]. Therefore, in this experiment, the most suitable imprinting ratio between template molecules and dual-hybrid functional monomers (AM-TEOSPI and MAA-APTES) was 1:4.

Synthesis of AT/MA-HMIPs

AM-TEOSPI and MAA-APTES have both the inorganic properties of silicon skeleton structure and the organic properties of AM and MAA (Supplementary Fig. S10). First, the double hybrid functional monomer reacts with the template molecule HCPT to form pre-polymerization (Fig. 2). MAA-APTES containing vinyl, silicate ester and acylamine groups, and siloxane functional monomer AM-TEOSPI with double hydrogen bond donor groups can interact with C=O, C=N, and C-N of the template molecule HCPT, and then through hydrogen bond polymerization, it is conducive to the selective capture of HCPT. The silicate ester in APTES generates silicon hydroxy, which is condensed with TEOS to generate a polymer skeleton so that the polymer has a more stable skeleton structure and can be more closely combined with template molecules [37]. Then, after the AIBN initiator was added, EGDMA was thermally induced by double bond-free radical polymerization, and HCPT and MAA were grafted onto the silicon skeleton to form a molecular imprinted layer supported by HCPT on the surface. The bifunctional monomers increase the binding sites of molecular imprinted materials, and the hard silicon skeleton structure effectively prevents the imprinted binding sites from being damaged, thus improving its adsorption capacity and reusability of HCPT. In order to remove HCPT, methanol-acetic acid

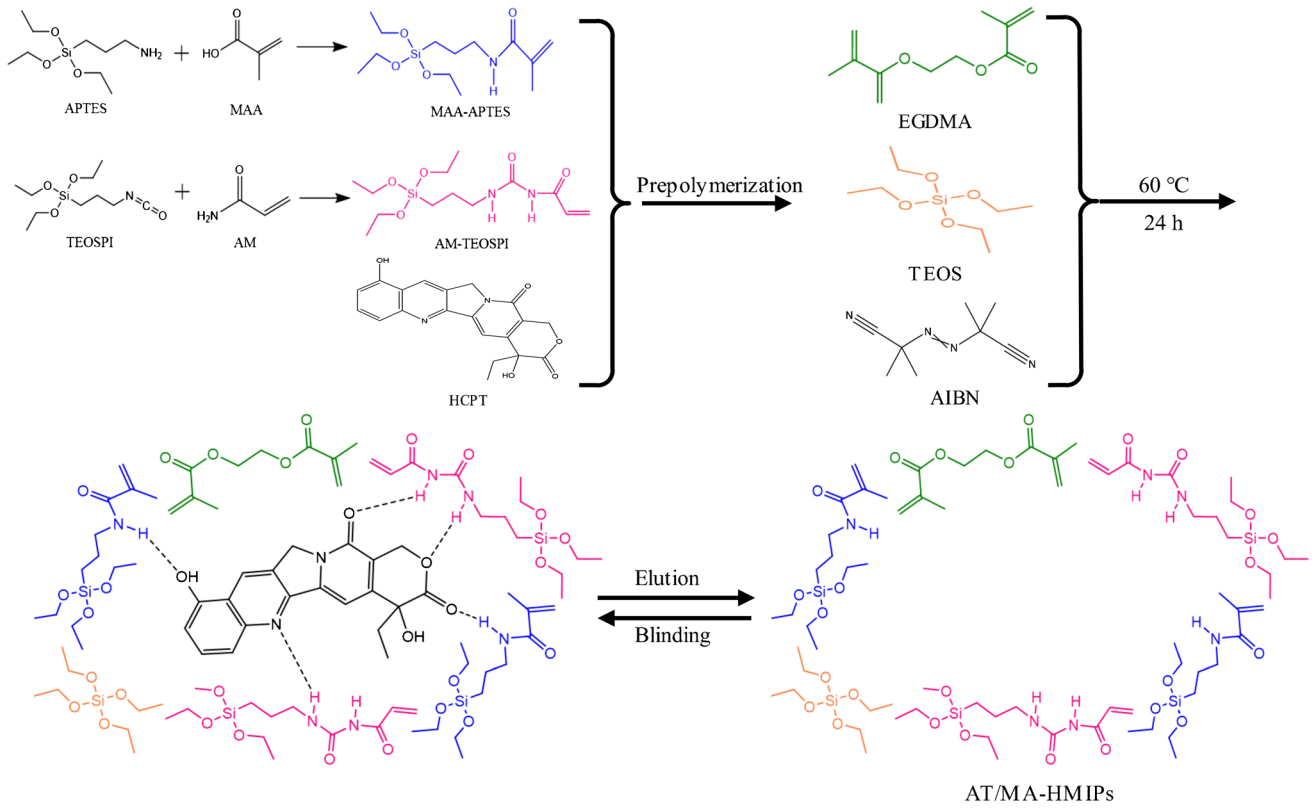

Fig. 2 Synthesis of AT/MA-HMIPs

(9:1, v/v) is used as the eluent. The acidic environment destroys the non-covalent force between the bifunctional monomer and HCPT, causing the release of the combined HCPT and resulting in a polymer with precisely arranged space holes and functional groups.

Characterizations

SEM-EDS analysis

The morphologies of AT/MA-HMIPs and AT/MA-HNIPs are irregular aggregates with compact morphology (Fig. 3). It can be found from Fig. 3E and Supplementary Fig. S11 and Table S3 that Si elements derived from AM-TEOSPI and MAA-APTES monomers are evenly distributed in the resulting AT/MA-HMIPs; it can conclude that AM-TEOSPI and MAA-APTES monomers have been successfully formed and well applied to the synthesis of AT/MA-HMIPs.

FTIR analysis

It is observed from Fig. 4A that the amide I band (1655 cm^{-1}), amide II band (1539 cm^{-1}), and amide III band (1255 cm^{-1}) correspond to the amide group in MAA-APTES and AM-TEOSPI. In addition, the characteristic peaks around 1390 cm^{-1} and 1157 cm^{-1} correspond to the tensile vibration of C=C and Si-O-Si in MAA-APTES, respectively, and the peak at 1726 cm^{-1} can be attributed to the tensile vibration of C=O in EGDMA [38]. The peak value at 947 cm^{-1} reflects the symmetric tensile vibration of Si-O-C. The vibration peak value of Si-O appears at 777 cm^{-1}. The small vibration peak at about 2956 cm^{-1} corresponds to the vibration of benzene ring C-H in AM-TEOSPI [37]. In addition, the two peaks at 1655 cm^{-1} and 1539 cm^{-1} can also be attributed to the vibration of C=O and N-H of AM-TEOSPI [39]. The appearance of small peaks may be due to the insufficient amount of functional monomers added in relation to the concentration of the polymer, and the infrared spectra of AT/MA-HNIPs and AT/MA-HMIPs are almost the same. It shows that the template molecule HCPT has been completely removed after elution, and the process of template molecule elution did not cause any changes in the composition of polymer functional groups [40]. Compared to AT/MA-HNIPs and AT/MA-HMIPs, the peaks of unwashed AT/MA-HMIPs at 1735 cm^{-1} and 1664 $cm^{-1}$are relatively weak and show a slight red shift, which may be due to the interaction between HCPT and MAA-APTES, AM-TEOSPI,

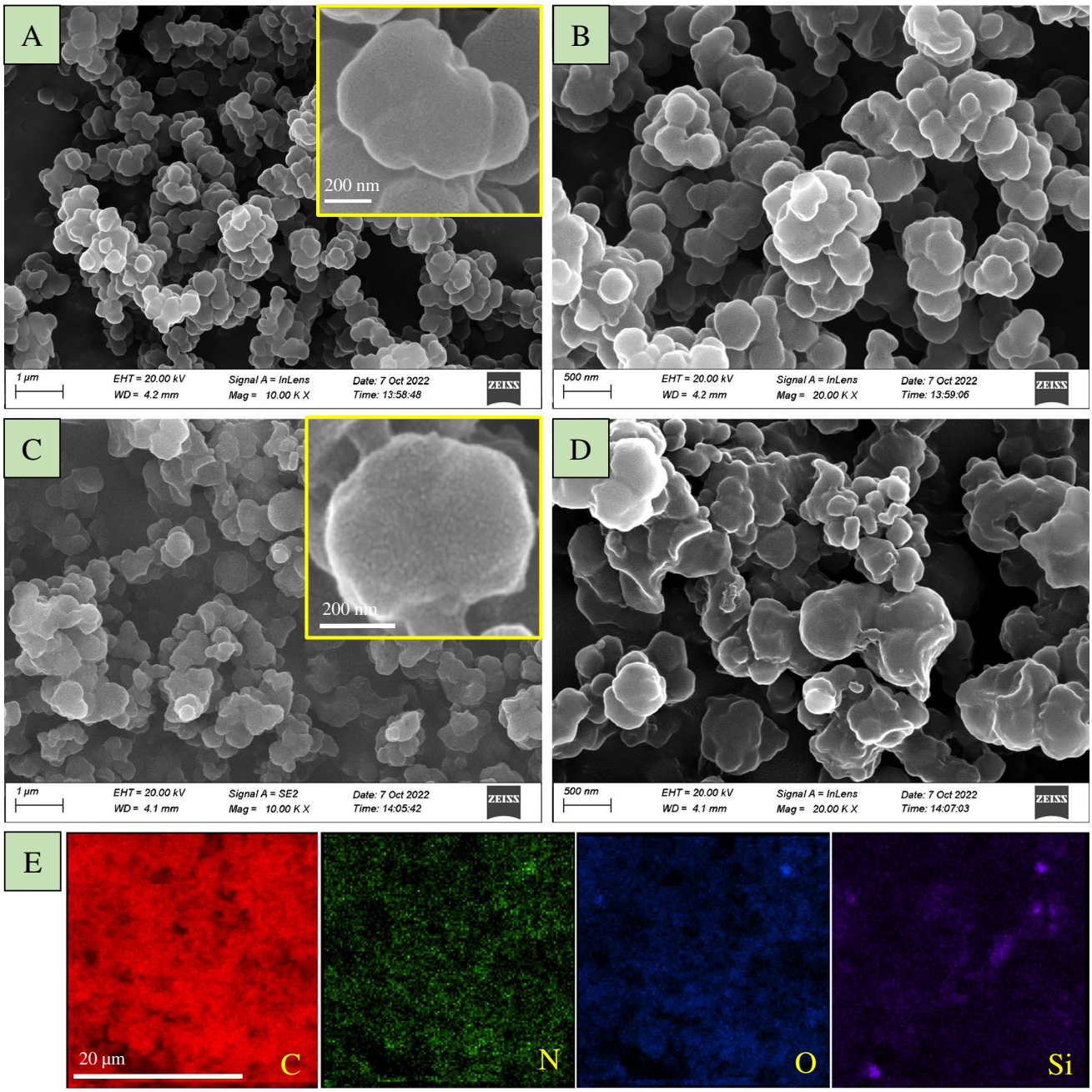

Fig. 3 SEM images of AT/MA-HMIPs: mag = 10,000× (**A**), mag = 20,000× (**B**); SEM images of AT/MA-HNIPs: mag = 10,000× (**C**), mag = 20,000× (**D**); EDS mapping of C, N, O, and Si (**E**)

indicating that HCPT has been successfully imprinted [41] [42]. The above results confirm that MAA-APTES, AM-TEOSPI, AT/MA-HMIPs, and AT/MA-HNIPs have been successfully prepared.

TGA analysis

As shown in Fig. 4B, the pyrolysis weight loss of AT/MA-HMIPs has four stages. In the first stage, the thermoweight loss of AT/MA-HMIPs is 0.55% in 40–120 °C. The weight

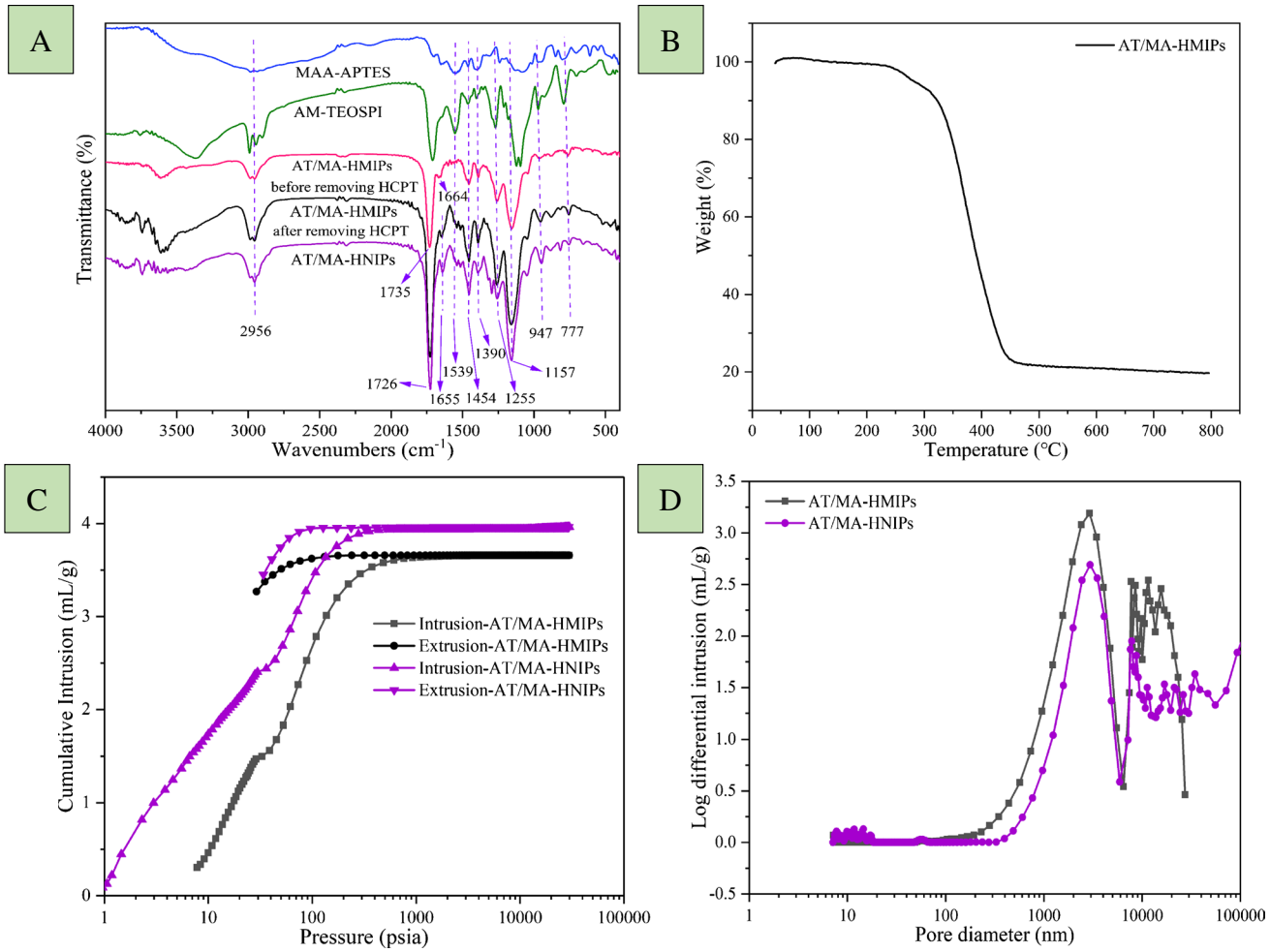

Fig. 4 FTIR spectra of AM-TEOSPI, MAA-APTES, AT/MA-HMIPs, and AT/MA-HNIPs (**A**); TGA curves of AT/MA-HMIPs and AT/MA-HNIPs (**B**); mercury extrusion/intrusion curves of AT/MA-HMIPs and AT/MA-HNIPs (**C**); pore size distribution curve of AT/MA-HMIPs and AT/MA-HNIPs (**D**)

loss of this part is mainly caused by the evaporation and loss of free water and bound water in the samples [43]. In the second stage, within the range of 120–270 °C, the curves of AT/MA-HMIPs tend to flatten out and there is basically no significant change in weight, which may be caused by the decomposition of small molecule polymers within this temperature range. In the third stage, the organic matter in the polymer undergoes a thermal decomposition reaction at 270–480 °C, and the weight loss of AT/MA-HMIPs reached the maximum value (78.04%). The organic matter is basically volatilized completely, indicating that the surface of AT/MA-HMIPs is basically wrapped by imprinted groups [44]. At the same time, it also shows that the prepared polymer cannot withstand a temperature above 270 °C. In 480–800 °C, the polymer basically decomposed completely.

MIP analysis

The mercury intrusion and extrusion curves of AT/MA-HMIPs and AT/MA-HNIPs showed good consistency (Fig. 4C), which means that each pore of the sample can be in direct contact with mercury or through larger pores [45]. Most of the pore sizes of AT/MA-HMIPs and AT/MA-HNIPs are mainly distributed between mesopores and macropores (Fig. 4D). Compared with AT/MA-HNIPs, the total pore volume, total pore area, and porosity of AT/MA-HMIPs are smaller, while the average pore size is larger (Supplementary Table S4). The thicker molecularly imprinted layer on the surface of AT/MA-HMIPs, combined with repeated elution of template molecules, may have contributed to the partial destruction of the pore structure.

Adsorption tests

Effect of pH

AT/MA-HMIPs have the highest adsorption capacity for HCPT, and it is significantly higher at pH 2–7 than at pH 8–10 (Fig. 5A). The decrease in adsorption capacity may be due to the dissociation of hydrogen bonds between template molecules and functional monomers under acidic conditions, resulting in the destruction of binding between AT/MA-HMIPs and HCPT [11]. When the pH value was 7, the maximum adsorption capacity was 15.58 ± 0.22 mg/g. The hydrogen bonding between HCPT and AT/MA-HMIPs is strong, which increases the adsorption capacity. When the pH value exceeds 8, the adsorption capacity is significantly reduced, which may be due to the instability of HCPT sodium salt and easy oxidative decomposition. The increase in the number of hydroxide ions weakened the hydrogen bonds between HCPT and AT/MA-HMIPs, resulting in a decreased adsorption capacity of 3.47 ± 0.20 mg/g. Compared with AT-HMIPs, MA-HMIPs, and MAA-MIPs, the higher adsorption capacity of AT/MA-HMIPs is attributed to the bifunctional hybrid monomer of the imprinted polymer, which has more adsorption sites and can better adsorb HCPT. So, the appropriate pH value selected for experiments was 7.

Adsorption isotherms

The results (Fig. 5B) show that AT/MA-HMIPs have better affinity for HCPT, and their adsorption capacity continues to increase with the increase of concentration until the

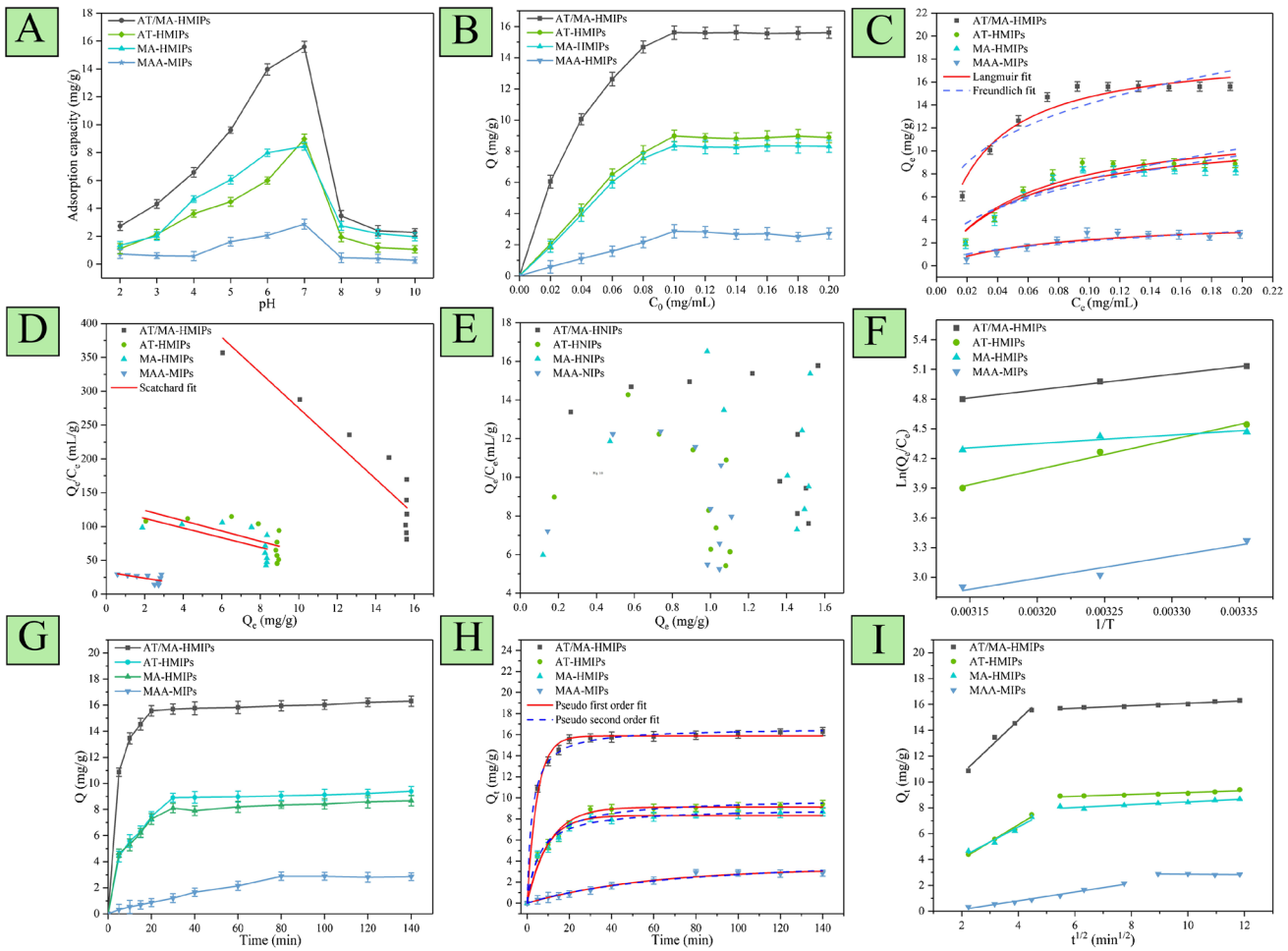

Fig. 5 Effect of pH on adsorption capacity (**A**); adsorption isotherm of AT/MA-HMIPs, AT-HMIPs, MA-HMIPs, and MAA-MIPs to HCPT (**B**); fitting curves of Langmuir and Freundlich models of HCPT on AT/MA-HMIPs, AT-HMIPs, MA-HMIPs, and MAA-MIPs (**C**); plot of ln*Kc* versus *1/T* on AT/MA-HMIPs, AT-HMIPs, MA-HMIPs, and MAA-MIPs (**D**); Scatchard plots of AT/MA-HMIPs, AT-HMIPs, MA-HMIPs, and MAA-MIPs (**E**); Scatchard plots of AT/MA-HNIPs, AT-HNIPs, MA-HNIPs, and MAA-MIPs (**F**); adsorption kinetic curve of HCPT (**F**); pseudo-first-order kinetic curves (**G**) and pseudo-second-order kinetic curves (**H**) of HCPT; fitting curve of intra-particle diffusion model for AT/MA-HMIPs, AT-HMIPs, MA-HMIPs, and MAA-MIPs adsorption on HCPT (**I**)

concentration is 0.10 mg/mL, reaching the saturation point, at which time the equilibrium adsorption capacity is 15.61 ± 0.17 mg/g. From Fig. 5C and Supplementary Table S5, we can see that the Langmuir model is more suitable for explaining its adsorption performance, and the adsorption of template molecule HCPT by AT/MA-HMIPs belongs to the chemical adsorption of the single molecular layer, indicating that the polymer surface is uniform, all adsorption sites are equivalent, and there is no interaction between the adsorbed molecular layers. Under certain conditions, a dynamic balance can be established between adsorption and desorption, and the probability of each molecule colliding with the solid surface to be adsorbed is certain [46].

The linear fitting of AT/MA-HMIPs is a straight line, indicating that they have a class of specific binding sites for HCPT (Fig. 5D). The Q_{max} of AT/MA-HMIPs is larger than AT-HMIPs, MA-HMIPs, and MAA-MIPs (Supplementary Table S6), indicating that the three-dimensional imprinted cavities formed during the synthesis of AT/MA-HMIPs have higher affinity [47]. On the contrary, the Scatchard curve of AT/MA-HNIPs, AT-HNIPs, MA-HNIPs, and MAA-NIPs in Fig. 5E is nonlinear, because there is no specific binding site on them and belongs to non-specific adsorption.

Adsorption thermodynamics

The curve (Fig. 5F) obtained by plotting $\ln K_c$ against $1/T$ has a good linear relationship. In addition, ΔH is negative (Supplementary Table S7), indicating that the adsorption of HCPT on the four polymers is an exothermic process [48]. The ΔS of AT/MA-HMIPs, AT-HMIPs, and MAA-MIPs is a negative value, which may be because the three recognize and adsorb HCPT through the imprinted cavity, and many HCPT molecules are adsorbed on the surface of polymer and enter the imprinted cavity, thus restricting the movement of HCPT in the imprinted cavity, reducing the degree of freedom, thus reducing the confusion of the whole recognition and adsorption system, and vice versa [49]. ΔG is negative, indicating that the adsorption of HCPT from solution to the surface of AT/MA-HMIPs, AT-HMIPs, MA-HMIPs, and MAA-MIPs is spontaneous, and the value of ΔG increased with higher temperature, which suggests that high temperature slowed the adsorption of HCPT on the polymer [50].

Adsorption kinetics

With the increase in adsorption time, the adsorption capacity of the four polymers on HCPT gradually increased and reached adsorption equilibrium at 20 min, 30 min, and 80 min, respectively (Fig. 5G). The AT/MA-HMIPs have a faster adsorption rate for HCPT, which may be due to the double hybrid monomer and sufficient imprinted cavity on its surface. In addition, with the further increase of adsorption time, the adsorption capacity of AT/MA-HMIPs did not fluctuate greatly, indicating that the silicon skeleton provided good support for it, so it had a more stable binding force.

As shown in Fig. 5H and Supplementary Table S8, the pseudo-second-order kinetic model is more suitable for explaining their dynamic adsorption behavior. The binding force between HCPT and polymer mainly depends on the hydrogen bond, hydrophobic interaction, and other forces formed between them, and more on the chemical adsorption process.

The adsorption processes of the four polymers are multilinear (Fig. 5I) because adsorption is controlled in many ways. There are two stages in the diffusion process of HCPT to AT/MA-HMIPs, AT-HMIPs, MA-HMIPs, and MAA-MIPs. In the first stage of rapid diffusion, a large number of HCPTs are rapidly adsorbed on the surfaces of AT/MA-HMIPs, AT-HMIPs, MA-HMIPs, and MAA-MIPs. When the adsorption sites on the surfaces are saturated, they begin to diffuse into the pores of the polymer and are adsorbed on the inner surface. The concentration of HCPT molecules decreases, and the adsorption of active sites on the inner surface of the polymer reaches a basic equilibrium, which is the second adsorption stage. The diffusion rate K_{3b} of HCPT decreases due to the resistance when HCPT diffuses into polymer pores in this stage. External and boundary diffusion processes may have also influenced the adsorption process, as evidenced by the non-zero intercept of the fitting curve [51, 52].

Adsorption selectivity

As shown in Fig. 6A and Supplementary Table S9, the adsorption capacity of AT/MA-HMIPs for HCPT (15.77 ± 0.24 mg/g) was significantly higher than that of CPT (2.31 ± 0.09 mg/g) and MCPT (2.03 ± 0.19 mg/g). It was about 6.83 and 7.77 times that of CPT and MCPT, respectively. AT/MA-HMIPs showed higher binding specificity to HCPT, and the results of imprinting factor α (10.73) also confirmed this (Supplementary Table S9). The high specificity of HCPT adsorption can be attributed to the presence of multiple imprinting recognition sites and hydrogen bonds on the surface of AT/MA-HMIPs. There was no significant difference in the adsorption of HCPT, CPT, and MCPT by MAA-MIPs, and the imprinting factor was only 2.43.

Method validation

When measuring a series of different concentrations of HCPT (Supplementary Table S10), a good linear relationship was obtained within 5–150 μg/mL (R^2 = 0.9988). When the signal-to-noise ratio (S/N) is 3 and 10, the LOD and LOQ are 0.339 μg/mL and 0.489 μg/mL, respectively. In the precision experiment, each concentration level was measured three times in parallel to obtain the peak area and

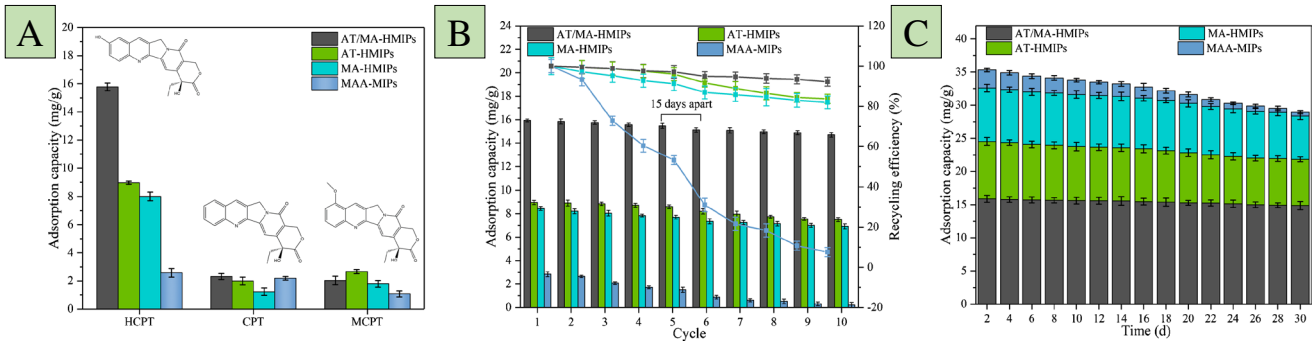

Fig. 6 Adsorptive capacity of AT/MA-HMIPs, AT-HMIPs, MA-HMIPs, and MAA-MIPs for HCPT, CPT, and MCPT and the chemical structure of HCPT, CPT, and MCPT (**A**); reusability of AT/MA-HMIPs, AT-HMIPs, MA-HMIPs, and MAA-MIPs (**B**); stability of AT/MA-HMIPs, AT-HMIPs, MA-HMIPs, and MAA-MIPs (**C**)

calculate the intra-day precision; measure once a day for three consecutive days to obtain the peak area and calculate the inter-day precision. The relative standard deviation (RSD) of both intra-day and inter-day measurements is less than 2.92%. Parallel experiments were conducted under optimal conditions; the RSD of HCPT content was determined to be 2.61%, indicating that the method has both high precision and accuracy based on the experimental results.

Reusability

The adsorption capacity of AT/MA-HMIPs, AT-HMIPs, MA-HMIPs, and MAA-MIPs decreases as the number of cycles increases (Fig. 6B), which may be attributed to the destruction of imprinting sites on their surfaces and pore plugging resulting from repeated adsorption-desorption cycles. After the sixth cycle, MAA-MIPs showed a significant reduction in adsorption capacity, as low as 0.88 ± 0.13 mg/g, possibly due to their poor structural stability in organic solvents. However, the adsorption capacity of AT/MA-HMIPs to HCPT only decreased by 7.75% after 10 adsorption-desorption cycles. The bifunctional monomers present on the surface of AT/MA-HMIPs serve as imprinting sites and maintain the original structure of the material due to their hard silicon skeleton, which helps reduce damage from external factors. Therefore, after 10 repeated adsorption and desorption cycles, AT/MA-HMIPs still maintain a high adsorption capacity (14.70 ± 0.31 mg/g) and recovery rate (92.25%) for HCPT, indicating that AT/MA-HMIPs have good reusability.

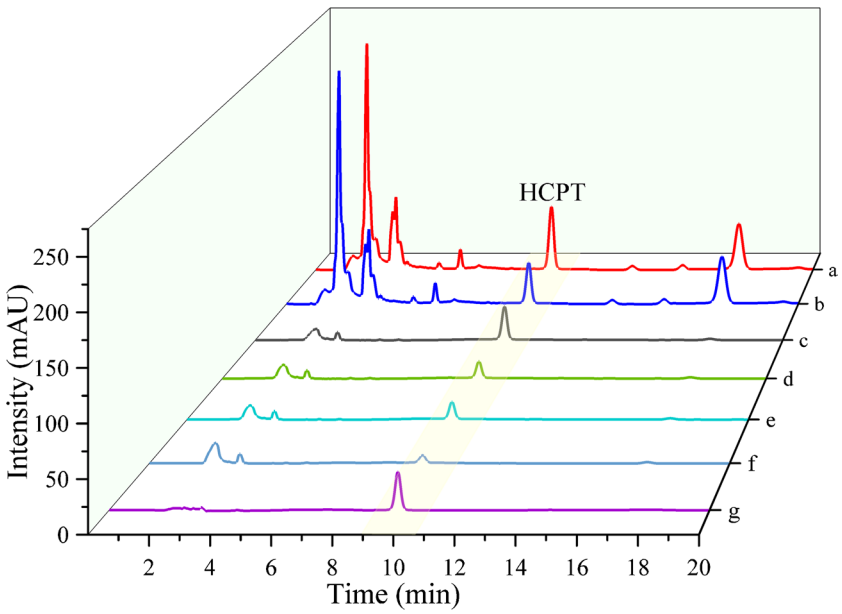

Fig. 7 Chromatogram of the crude extract of *C. camptotheca* seeds before adsorption using adsorbent (**a**); chromatogram of crude extract from *C. camptotheca* seeds after adsorption with adsorbent (**b**); chromatogram of the desorption solution after adsorption using AT/MA-HMIPs (**c**); chromatogram of the desorption solution after adsorption using AT-HMIPs (**d**); chromatogram of the desorption solution after adsorption using MA-HMIPs (**e**); chromatogram of desorption solution after adsorption using MAA-MIPs (**f**); after purification using an AT/MA-HMIPs solid phase extraction column, the desorption solution chromatogram is obtained (**g**)

Table 1 Comparison with previously reported other adsorbents for HCPT adsorption capacity

Adsorbents	Usage amount (mg)	Volume (mL)	Equilibrium time (h)	Adsorption capacity (mg/g)	Desorption agent	Imprinting factor	Purity (%)
AT/MA-HMIPs	5.0	10	0.33	15.77 ± 0.24	Methanol-acetic acid (9:1)	10.73	80.86
AT-HMIPs	5.0	10	0.5	8.97 ± 0.19	Methanol-acetic acid (9:1)	5.64	40.22
MA-HMIPs	5.0	10	0.5	8.01 ± 0.33	Methanol-acetic acid (9:1)	5.38	38.25
MAA-MIPs	5.0	10	1.33	2.58 ± 0.16	Methanol-acetic acid (9:1)	2.43	29.63
CMC/GO@MIPs [11]	5.0	10	0.5	57.56	Methanol-acetic acid (9:1)	2.60	50.94
Macroporous resin (AB-8) [55]	3000	100	7	14.37	Ethanol (70%)	-	21.00
Macroporous resin (X-5) [56]	500	100	4	16.50	Ethanol (70%)	-	7.19

Stability

The adsorption capacity of AT-HMIPs and MA-HMIPs remained relatively stable in the first 16 d, and then the downward trend was more obvious (Fig. 6C). On the 16th day, the adsorption capacity of AT-HMIPs and MA-HMIPs to HCPT gradually decreased to 7.92 ± 0.35 mg/g and 7.65 ± 0.20 mg/g, respectively. However, AT/MA-HMIPs have maintained a high adsorption capacity, indicating that AT/MA-HMIPs can maintain their own structure for a long time and have a stable adsorption capacity. The adsorption capacity and adsorption efficiency were reduced by 1.09 mg/g and 6.82%, separately.

SPE application of AT/MA-HMIPs in crude extract of *C. camptotheca* seeds

Optimization of SPE procedures is described in Part S6 in the Supplementary information. As shown in Fig. 7, there are many impurity peaks in the solution before adsorption (curve a). After the HCPT is targeted and adsorbed with AT/MA-HMIPs, it can be observed that the peak of HCPT is significantly reduced, and the peak of other impurities is almost unchanged (curve b). The eluted HPLC chromatogram has a high HCPT peak and a small amount of impurities (curve c). In addition, the HCPT peaks after elution of AT-HMIPs, MA-HMIPs, and MAA-MIPs decreased in turn, and the adsorption effect was not as good as that of AT/MA-HMIPs. These results indicate that HCPT can be separated and purified more effectively by using AT/MA-HMIPs. Curve g is the HPLC chromatogram after using the SPE column for extraction. It can be clearly seen that the chromatogram after using the SPE column is cleaner than that before using the SPE column, with almost no impurity peaks. This indicates that the purity of HCPT has been further improved after using the SPE column. HPLC analysis at 254 nm detected a concentration of 5.76 mg/L of HCPT in the eluent. The eluent was dried by rotary evaporation and weighed, and the purity of HCPT was calculated as 80.86%; the yield was 61.43%. The excellent selectivity and affinity of AT/MA-HMIPs for HCPT demonstrate their potential for successful separation and purification of HCPT from *C. camptotheca* seeds.

Comparison of relevant adsorbents

The purity of the two macroporous resins for HCPT is much lower than that of AT/MA-HMIPs prepared in this study (Table 1). At the same dosage, the amount needed for the experiment was 60 and 10 times that of AT/MA-HMIPs, and the extraction and desorption process consumed large amounts of ethanol, which caused high costs. In addition, the AT/MA-HMIPs prepared in this study have a shorter enrichment time (0.33 h) compared to other MIPs and macroporous resins, as the double hybrid monomers make AT/MA-HMIPs more abundant in functional groups, and the application of surface imprinting can effectively avoid the phenomenon of binding site embedding and rapid mass transfer, indicating the potential of AT/MA-HMIPs in efficient enrichment of HCPT [53]. Compared with the other three MIPs prepared in this test, AT/MA-HMIPs have a higher imprinting factor (10.73), which means that the targeted adsorption of HCPT is superior and more effective. The large imprinting factor values of AT/MA-HMIPs indicate that double hybrid monomer molecularly imprinted materials have enormous extraction and purification potential, and this high selectivity has broad development prospects in this field [54]. Therefore, the obtained AT/MA-HMIPs are expected to serve as efficient adsorbents for selective separation and determination of HCPT from complex matrices.

Conclusions

With the assistance of computer molecular simulation, this study synthesized HCPT MIPs with excellent adsorption capacity, reusability, stability, and selectivity using hybrid monomers MAA-APTES and AM-TEOSPI as dual

monomers and successfully separated and enriched HCPT in *C. camptotheca*. This study not only provides new ideas for the designability and selectivity of hybrid monomers in molecular imprinting synthesis but also has broad application prospects in the effective separation of bioactive compounds in natural plants, food, or pharmaceutical industries. Although the adsorption capacity of AT/MA-HMIPs is not high enough, it is worth noting that AT/MA-HMIPs have advantages such as high purity and short equilibrium time. In addition, the recent research trend is to improve its performance by adding some metal skeleton materials or additional functional groups, which may further enhance its adsorption capacity.

Supplementary Information The online version contains supplementary material available at https://doi.org/10.1007/s00604-023-05997-4.

Acknowledgements The National Key Research and Development Project of China (2022YFD2200805), the Fundamental Research Fund for Central Universities (2572022DP06), Heilongjiang Touyan Innovation Team Program (Tree Genetics and Breeding Innovation Team), and the 111 Project, China (B20088).

Declarations

Conflict of interest The authors declare no competing interests.

References

1. Zhao CJ, Zhang YK, Li CY, He X, Yang L, Fu Y et al (2016) Development of an ionic liquid-based ultrasonic/microwave-assisted simultaneous distillation and extraction method for separation of camptothecin, 10-hydroxycamptothecin, vincoside-lactam, and essential oils from the fruits of *Camptotheca acuminata* Decne. Appl Sci 6(10):293
2. Wang T, Li PF, Sun Y, Song XM, Li H, Qin LT et al (2020) Camptothecin-imprinted polymer microspheres with rosin-based cross-linker for separation of camptothecin from *Camptotheca acuminata* fruit. Sep Purif Technol 234:116085
3. Hu WC, Zhao YQ, Yang Y, Zhang HF, Ding CB, Hu C et al (2019) Microwave-assisted extraction, physicochemical characterization and bioactivity of polysaccharides from *Camptotheca acuminata* fruits. Int J Biol Macromol 133:127–136
4. Guo YY, Gao T, Fang F, Sun S, Yang DY, Li YJ et al (2021) A novel polymer micelle as a targeted drug delivery system for 10-hydroxycamptothecin with high drug-loading properties and anti-tumor efficacy. Biophys Chem 279:106679
5. Zhang QL, Liu LH, Ni YN (2022) Magnetic reduced graphene oxide (MrGO) nanocomposites as nano carries for loading and transferring of 10-hydroxycamptothecin. J Mol Liq 362:119680
6. Wang YT, Xuan JJ, Zhao GC, Wang DD, Ying N, Zhuang J (2021) Improving stability and oral bioavailability of hydroxycamptothecin via nanocrystals in microparticles (NCs/MPs) technology. Int J Pharm 604:120729
7. Cui GQ, Yang XB, Liu TT, Liu ZZ, Yang L (2018) An efficient approach for the enzyme-enhanced extraction of camptothecin and 10-hydroxycamptothecin from the samara of *Camptotheca acuminata* using an ionic liquid solution. Sep Purif Technol 200:102–111
8. Teixeira SPB, Reis RL, Peppas NA, Gomes ME, Domingues RMA (2021) Epitope-imprinted polymers: design principles of synthetic binding partners for natural biomacromolecules. Sci Adv 7(44):eabi9884
9. Li CY, Nie F, Feng CY, Tian MF, Yu MT, Zhao CJ et al (2022) Magnetic dual-template molecularly imprinted polymers for separation and enrichment of echinacoside and acteoside from *Cistanche deserticola* YC Ma. Chem Eng Res Des 182:719–732
10. Li XT, Wan JQ, Wang Y, Yan ZC, Chi HY, Ding S (2020) Mechanism of accurate recognition and catalysis of diethyl phthalate (DEP) in wastewater by novel MIL100 molecularly imprinted materials. Appl Catal B-Environ 266:118591
11. Nie F, Li CY, Ahmad N, Yuan ZY, Tan YL, Xu YW et al (2022) Molecularly imprinted polymer based on carboxymethylcellulose/graphene oxide composites for selective adsorption of hydroxycamptothecin. Acs Appl Polym Mater 4(12):9294–9304
12. Ayankojo AG, Reut J, Öpik A, Furchner A, Syritski V (2018) Hybrid molecularly imprinted polymer for amoxicillin detection. Biosens Bioelectron 118:102–107
13. Wei ZH, Zhang RR, Mu LN, Huang YP, Liu ZS (2019) Fabrication of core-shell sol-gel hybrid molecularly imprinted polymer based on metal–organic framework. Eur Polym J 121:109301
14. Da Silva AS, De Oliveira HL, Da Silva ATM, Do Nascimento TA, Borges KB (2017) Preparation of an organic–inorganic hybrid molecularly imprinted polymer for effective removal of albendazole sulfoxide enantiomers from aqueous medium. J Environ Chem Eng 5(6):6179–6187
15. Tang WY, Li GZ, Row KH, Zhu T (2016) Preparation of hybrid molecularly imprinted polymer with double-templates for rapid simultaneous purification of theophylline and chlorogenic acid in green tea. Talanta 152:1–8
16. Yang X, Wang RL, Wang WH, Yan HY, Qiu MD, Song YX (2014) Synthesis of a novel molecularly imprinted organic–inorganic hybrid polymer for the selective isolation and determination of fluoroquinolones in tilapia. J Chromatogr B 945-946:127–134
17. Yan HY, Wang MY, Han YH, Qiao FX, Row KH (2014) Hybrid molecularly imprinted polymers synthesized with 3-aminopropyltriethoxysilane-methacrylic acid monomer for miniaturized solid-phase extraction: a new and economical sample preparation strategy for determination of acyclovir in urine. J Chromatogr A 1346:16–24
18. Gao J, Yan L, Yan Y, Chen L, Lu J, Xing WD et al (2022) Solvent-driven controllable molecularly imprinted membrane with switched selectivity and fast regenerability enabled by customized bifunctional monomers. Chem Eng J 446:136991
19. Lu H, Liu MM, Cui HY, Huang Y, Li L, Ding YP (2022) An advanced molecularly imprinted electrochemical sensor based bifunctional monomers for highly sensitive detection of nitrofurazone. Electrochim Acta 427:140858
20. Li YG, Zhang L, Dang YY, Chen ZQ, Zhang RY, Li YC et al (2019) A robust electrochemical sensing of molecularly imprinted polymer prepared by using bifunctional monomer and its application in detection of cypermethrin. Biosens Bioelectron 127:207–214
21. Zhang JW, Tan L, Yuan JB, Qiao RF, Wang CZ, Yang FQ et al (2020) Extraction of activated epimedium glycosides in vivo and in vitro by using bifunctional-monomer chitosan magnetic molecularly imprinted polymers and identification by UPLC-Q-TOF-MS. Talanta 219:121350
22. Huang YF, Li YY, Wu YF, Huang XJ (2023) Computer-aided design-based green fabrication of magnetic molecularly imprinted nanoparticles for specific extraction of non-steroidal anti-inflammatory drugs. Chem Eng J 452:139440
23. Pan D, Zhu KF, Zhang YZ, Sun LX, Hao XH (2022) First principles and molecular dynamics simulation investigation of

mechanical properties of the PTFE/graphene composites. Compos Part B-Eng 242:110050
24. Zhang PA, Yuan JM, Pang AM, Tang G, Deng JR (2020) A novel UV-curing liner for NEPE propellant: insight from molecular simulations. Compos Part B-Eng 195:108087
25. Frisch A, Hratchian HP, Dennington RD, Keith TA, Millam J, Nielsen B, et al. (2009) Gaussview 6.0. 8.
26. Frisch MJ, Trucks GW, Schlegel HB, Scuseria GE, Robb MA, Cheeseman JR et al (2016) Gaussian 16. Gaussian, Inc., Wallingford, CT
27. Grimme S, Ehrlich S, Goerigk L (2011) Effect of the damping function in dispersion corrected density functional theory. J Comput Chem 32(7):1456–1465
28. Lu T, Chen FW (2012) Multiwfn: a multifunctional wavefunction analyzer. J Comput Chem 33(5):580–592
29. Lu T, Chen QX (2022) Independent gradient model based on Hirshfeld partition: a new method for visual study of interactions in chemical systems. J Comput Chem 43(8):539–555
30. Humphrey W, Dalke A, Schulten K (1996) VMD: visual molecular dynamics. J Mol Graph Model 14(1):33–38
31. Zu YG, Zhao CJ, Fu YJ, Li QY, Li CY (2004) Determination of camptothecin and hydroxycamptothecin by high performance liquid chromatography with changing detection wavelength. Anal Chem 32(11):1441–1444
32. Ma YM, Jiang MW, Liu XJ, Xu XY, Jiang XX, Chen LG et al (2022) Functionally modified cross-linked molecularly imprinted resins: separation and purification of camptothecin and its theoretical study. Ind Crop Prod 184:115078
33. He YQ, Fudickar W, Tang JH, Wang H, Stang PJ (2020) Capture and release of singlet oxygen in coordination-driven self-assembled organoplatinum(II) metallacycles. J Am Chem Soc 142(5):2601–2608
34. Xian WW, Yi K, Jun PJ, Bin L, Fei XH (2022) Probing the mechanism of green solvent solubilization of hemicellulose based on molecular dynamics simulations. Ind Crop Prod 186(186):115159
35. Ling X (2009) Synthesis, characterization and application of molecularly imprinted polymer nanospheres. Sichuan Normal University
36. Wang XG, Liu ZX, Lu J, Teng HH, Fukuda H, Qin WD et al (2022) Highly selective membrane for efficient separation of environmental determinands: enhanced molecular imprinting in polydopamine-embedded porous sleeve. Chem Eng J 449:137825
37. Tan L, Guo ML, Tan J, Geng YY, Huang SY, Tang YW et al (2019) Development of high-luminescence perovskite quantum dots coated with molecularly imprinted polymers for pesticide detection by slowly hydrolysing the organosilicon monomers in situ. Sensor Actuat B-Chem 291:226–234
38. Shao HK, Zhou HB, Zhang TT, Zhao XL, Jiang ZJ, Wang QQ (2019) Preparation of molecularly imprinted hybrid monoliths for the selective detection of fluoroquinolones in infant formula powders. J Chromatogr A 1588:33–40
39. Cai XQ, Li JH, Zhang Z, Yang FF, Dong RC, Chen LX (2014) Novel Pb^{2+} ion imprinted polymers based on ionic interaction via synergy of dual functional monomers for selective solid-phase extraction of Pb^{2+} in water samples. ACS Appl Mater Interfaces 6(1):305–313
40. da Mata K, Corazza MZ, de Oliveira FM, de Toffoli AL, Tarley CRT, Moreira AB (2014) Synthesis and characterization of cross-linked molecularly imprinted polyacrylamide for the extraction/preconcentration of glyphosate and aminomethylphosphonic acid from water samples. React Funct Polym 83:76–83
41. Li HH, Zhang WC, Wu ZY, Huang XS, Hui AL, He YW et al (2020) Theoretical design, preparation, and evaluation of Ginkgolide B molecularly imprinted polymers. J Sep Sci 43(2):514–523
42. Ma Y, Mao CY, Du XD, Xie CS, Zhou JM, Tao XQ et al (2023) Insight into the application of magnetic molecularly imprinted polymers in soil-washing effluent: selective removal of 4, 4′-dibromodiphenyl ether, high adaptivity of material and efficient recovery of eluent. Chemosphere 334:138990
43. Nanicuacua DM, Gorla FA, de Almeida SM, Segatelli MG, Tarley CRT (2022) Synthesis of a novel bifunctional hybrid molecularly imprinted poly (methacrylic acid-phenyltrimetoxysilane) for highly effective adsorption of diuron from aqueous medium. React Funct Polym 181:105432
44. Bhogal S, Mohiuddin I, Kim KH, Malik AK, Kaur K (2023) Restricted access medium magnetic molecularly imprinted polymers: validation of their suitability as an effective quantitation tool against phthalates in food products packaged in plastic. Chem Eng J 457:141270
45. Zhu ZQ, Niu Y, Wang S, Su M, Long Y, Sun HX et al (2022) Magnesium hydroxide coated hollow glass microspheres/chitosan composite aerogels with excellent thermal insulation and flame retardancy. J Colloid Interface Sci 612:35–42
46. Xing WD, Ma ZF, Wang C, Gao J, Yu C, Yan YS et al (2023) Hierarchically porous molecularly imprinted membranes with multiple transfer channels for micropollutants selective separation. Desalination 547:116226
47. Fan L, Zhang Q, Wang F, Hf Y (2023) Dummy molecularly imprinted solid-phase extraction-SERS determination of AFB1 in peanut. Spectrochim Acta A 288:122130
48. Qu Y, Qin L, Guo MC, Liu XG, Yang YZ (2022) Multilayered molecularly imprinted composite membrane based on porous carbon nanospheres/pDA cooperative structure for selective adsorption and separation of phenol. Sep Purif Technol 280:119915
49. Yang XX, Muhammad T, Yang JJ, Yasen A, Chen LX (2020) In-situ kinetic and thermodynamic study of 2, 4-dichlorophenoxyacetic acid adsorption on molecularly imprinted polymer based solid-phase microextraction coatings. Sensor Actuat A-Phys 313:112190
50. Zheng XD, Sun W, Li A, Zhang YZ, Li ZY (2022) Bacterial cellulose nanofibrous ion imprinted aerogel for highly efficient recognition and adsorption of Dy (III). Process Saf Environ 160:70–79
51. Wang LH, Zhang CY, Chen YJ, Deng QL, Wang S (2020) Dummy molecularly imprinted silica materials for effective removal of aristolochic acid I from kaempfer dutchmanspipe root extract. Microchem J 152:104463
52. Shi SY, Fan DX, Xiang HY, Li HA (2017) Effective synthesis of magnetic porous molecularly imprinted polymers for efficient and selective extraction of cinnamic acid from apple juices. Food Chem 237:198–204
53. Yang LL, Li T, Yang DD, Li YJ, He JY, Zhou LD et al (2023) Constructing a dummy-template adsorbent using magnetic molecular-imprinted chitosan for rapid enrichment of flavonoids compounds from Penthorum chinense Pursh. Microchem J 191:108833
54. Lafarge C, Bitar M, El Hosry L, Cayot P, Bou-Maroun E (2020) Comparison of molecularly imprinted polymers (MIP) and sol–gel molecularly imprinted silica (MIS) for fungicide in a hydro alcoholic solution. Mater Today Commun 24:101157
55. Yang JH (2020) Study on extraction of Camptothecin and 10-hydroxycamptothecin from *Camptotheca acuminata* Decne leaves and new technology for separation and purification of 10-hydroxycamptothecin. Northeast Forestry University
56. Li JH (2009) Study on extraction and separation of main alkaloids from *Camptotheca acuminata*. Northeast Forestry University